

# Wind Forces in Overgrown Rope Façades

## Wind Tunnel Tests on Five Climbing Plants

**Kilian Arnold\*, Susanne Gosztonyi, Andreas Luible**

\* Corresponding author

Lucerne University of Applied Sciences and Arts Engineering and Architecture, kilian.arnold@hslu.ch

### Abstract

*Overgrown rope façades offer a space-saving possibility to make cities greener while counteracting the effect of the urban heat island (UHI). Unfortunately, there are no design models that adequately characterise the interaction between wind and plants for the calculation of wind loads. In the preceding study about overgrown rope façades (Arnold et al., 2021), a design model was deduced from flow force studies on trees and a drag coefficient for plants on overgrown rope façades was derived from drag resistance measurements of deciduous trees. This drag coefficient has not been validated. In this study, wind load tests in a turbulent wind tunnel were performed on five climbing plants to validate the drag coefficient. For this purpose, a prototype of a turbulent wind tunnel with an active grid that simulates gusts for a chaotic turbulent flow was built and various overgrown rope samples were measured. Based on the measured data, the 95% characteristic value of the drag coefficients was calculated using a statistical method. These drag coefficients can be applied to buildings at different speeds by means of E-values and B-values, thus allowing the design optimisation of plant climbing systems. This work does not deal with the interaction between the façade surface and overgrown rope plant in front of the façade, which requires further research.*

### Keywords

*green façades, wind forces, overgrown rope façades, drag coefficient, climbing plants, urban greenery, UHI, wind tunnel testing, active grid*

10.7480/jfde.2021.2.4833

# 1 INTRODUCTION

For vertical green systems, three other greening approaches exist besides the ground-based (direct) vegetation (e.g. ivy) (1); "Overgrown rope façades" (2); "balcony boxes greening systems" (3); and "living wall" – a wall-based surface greening (4), (Pfoser, 2016) (see Figure 1).

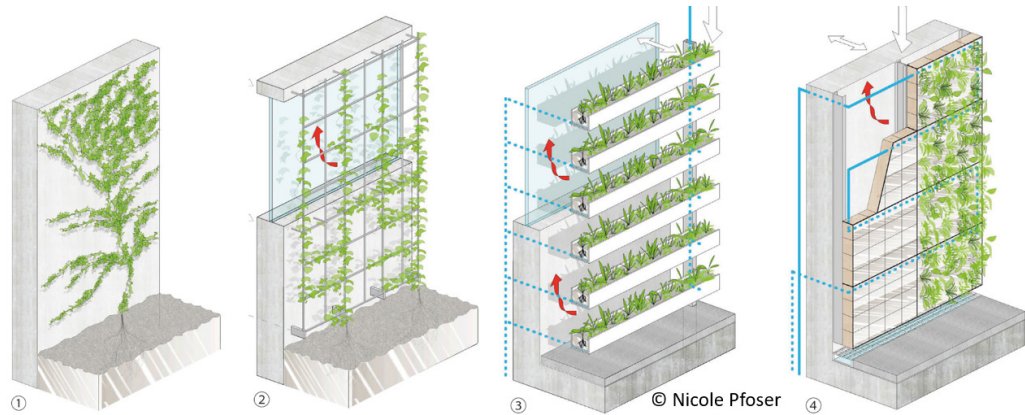


FIG. 1 Different vertical green systems:1) ground-based, 2) overgrown rope façades, 3) balcony boxes system, 4) living wall. (Pfoser 2016, p. 126-127, Figure 137) & (Pfoser 2018, p. 166-167)

This paper focuses on the "overgrown rope façades" type since this vertical greening system belongs to the category of wind flow-through systems. The plants on the rank constructions are exposed to direct wind currents on the building.

In the first part of the study on overgrown rope façades, studies on drag coefficients for plants were reviewed and the critical parameters for drag coefficients for overgrown rope façades were identified (Arnold et al., 2021). Eight academic articles and one set of guidelines with high relevance were analysed in greater detail, because they had measured the airflow resistance on deciduous or fir trees (or individual leaves) based on wind tunnel or field tests. Moreover, the guidelines provide reduction factors (drag coefficients) for wind load calculation on plants for overgrown rope façades. For calculation of the wind forces for plants in overgrown rope façades, a design model was derived from this study review by Arnold et al. (2021) based on a drag coefficient that is dynamic, as given in formula (1.1). The drag coefficient  $C_D$  for plants is a product of a constant (B-value) multiplied by the speed raised to a further constant (E-value).

$$c_D = B \cdot v^E \quad [-] \quad (1.1)$$

The model was verified based on the test results in the selected representative studies. Furthermore, a possible drag coefficient for plants on overgrown rope façades was derived from the reviewed studies according to formula (1.2)

$$c_D = 3.92 \cdot v^{-0.63} \quad [-] \quad (1.2)$$

Using this formula or drag coefficient, the resultant flow forces can be calculated for overgrown rope façades at any wind speed.

Since formula (1.2) is based on the results of the reviewed wind load tests for deciduous trees, it is to be assumed that plants for overgrown rope façades on buildings with their shell-like structure absorb significantly lower wind loads compared to free-standing deciduous trees. It is thus to be further assumed that higher wind loads are determined with this drag coefficient compared to what actually occurs with climbing plants on overgrown rope façades, thereby providing design safety.

The objective of this article is to check and validate the derived drag coefficient of Arnold et al. (2021) based on the test results of Arnold (2018). The effects between the façade construction and the overgrown rope layis are not considered for this goal.

In order to perform measurements on plants of this type, it was first necessary to develop an entirely turbulent wind tunnel capable of simulating wind turbulences and gusts. This wind tunnel prototype was validated based on comparison measurements. It was likewise necessary to develop a suitable measurement and evaluation methodology for the measurement results. Following the set-up and validation of the test environment, the drag resistance measurements on five climbing plants were performed and the proposed drag coefficients evaluated. Figure 2 illustrates the two-track procedure applied in the work.



FIG. 2 Two-track procedure in study

The requirements for the wind tunnel are discussed in section 2 along with the physical fundamentals underlying wind flows. Then, the prototype of a turbulent wind tunnel with the measurement settings and comparison measurement for validating the wind tunnel are also briefly presented in this section. Section 3 describes the plant samples, the measurement methodology and evaluation process, while section 4 presents the results followed by a discussion thereof in section 5.

## 2 SET-UP OF THE WIND TUNNEL

### 2.1 THEORY: PHYSICAL PRINCIPLES OF WIND

Load determination in Switzerland is carried out based on the Swiss SIA standards. These standards contain the occurring wind speed in Switzerland based on the dynamic pressure. The highest reference value for the dynamic pressure  $q_p$  in the lowlands of Switzerland is equal to 1300 Pascal (SIA 261:2014, Appendix E). Based on the design method from SIA 261, Chapter 6, the dynamic pressure can be converted for the building location and building shape to allow determination of the effective wind loads on façades. Using formula (2.1) from Hertig & Zimmrli, (2006), the dynamic pressure can be converted into the peak speed of a gust:

$$\hat{v} = \sqrt{\frac{2 \cdot q_p}{\rho_A}} = \sqrt{\frac{2 \cdot 1300 \cdot Pa}{1.225 \cdot \frac{kg}{m^3}}} = 46 \text{ m/s} \quad (2.1)$$

Here,  $\hat{v}$  is the peak speed of the gust,  $q_p$  the dynamic pressure and  $\rho_A$  the density of the air. The peak speed of the gust can be converted using the gust factor  $G_v$  according to formula (2.2) to the average speed  $v_m$ . In Switzerland, a gust factor of 1.9 is applicable (Hertig & Zimmerli, 2006).

$$v_m = \frac{\hat{v}}{G_v} = \frac{46 \text{ m/s}}{1.9} = 24.2 \text{ m/s} \quad (2.2)$$

Based on the standard deviation of the speed measurement over a time interval, the irregular speeds of the wind profile can be mathematically characterised. Dividing the standard deviation of the speed measurement by the average speed, the turbulence intensity  $I$ , is obtained, which is defined according to formula (2.3) (Hertig & Zimmerli, 2006).

$$I = \frac{\sigma}{v_m} = \frac{\sqrt{\Delta \bar{v}^2}}{v_m} = \frac{\sqrt{\frac{1}{T} \int_0^T (v(t) - v_m)^2 dt}}{v_m} \quad [-] \quad (2.3)$$

The turbulence intensities of the natural wind profile on the earth's surface vary depending on the height. The turbulence intensities are also dependent on the roughness of the earth's surface. For the different roughness profiles in Switzerland, the turbulence intensities of the Prandtl layer are depicted in Figure 3. In the building height range from 5m to 40m, the turbulence values are between 20% and 40%.

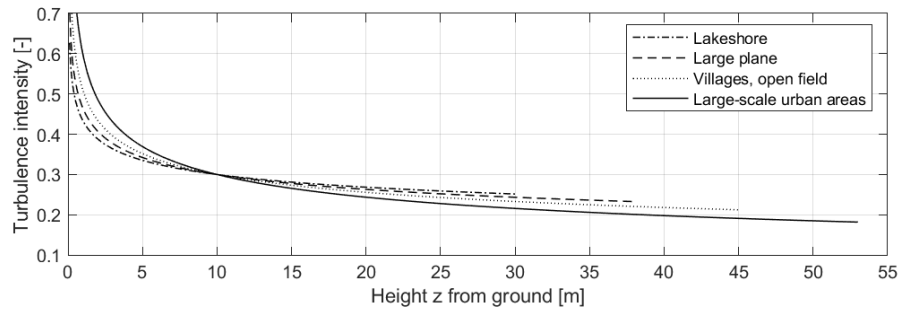


FIG. 3 Turbulence intensities of the Prandtl layer in different regions

Climbing plants can attain growth heights of up to 30 meters (Pfoser, 2016). Overgrown rope façades are placed on buildings in this fully turbulent Prandtl layer with turbulence intensities from 20% to 40%.

## 2.2 WIND TUNNEL DEVELOPMENT

In the first study, (Arnold et al., 2021), research was carried out on plants after wind load tests. Studies were found mainly of wind tunnel tests in a laminar flow, as well as tests with pick-ups, in which the samples were driven over a distance to gain wind flow patterns. If a body is moved through a standing air mass, the air mass creafloes laminar flow around it. Most of the studies were therefore carried out in laminar flow profiles.

Based on these results and the physical principles of wind in subsection 2.1, it was decided to develop a turbulent, Eiffel-type wind tunnel that allows wind force tests to be performed in a turbulent, gusty flow profile on climbing plants for overgrown rope façades. Wind load determinations on buildings are usually carried out in a boundary layer wind tunnel. The atmospheric boundary layer is scaled to the tunnel height. The test specimen must be scaled down to the same scale (Cook, 1975). To produce the plant samples with their properties as a model on a small scale is very difficult and almost impossible, so the investigation was done in a fully turbulent wind tunnel. Eiffel's design (Chanetz, 2017) features a simple arrangement of the wind tunnel that has the benefit of expelling contamination or torn leaves out of the tunnel. Due to the atypical positioning of the ventilator at the air intake, the ventilator is protected against torn-off plant parts.

The wind tunnel (Figure. 4) has a total length of 15m and a flow cross-section of 1m x 1.5m (W x H). The measuring section has a cross-section of 1m x 1m and a length of 3m. Prior to the measuring section, the tunnel is tapered over 3m to the cross-section of the measuring section. Due to the tapering, the flow is accelerated, thereby producing higher air speeds in the measuring section. Figure 4 shows the wind tunnel set-up with a flow simulation.

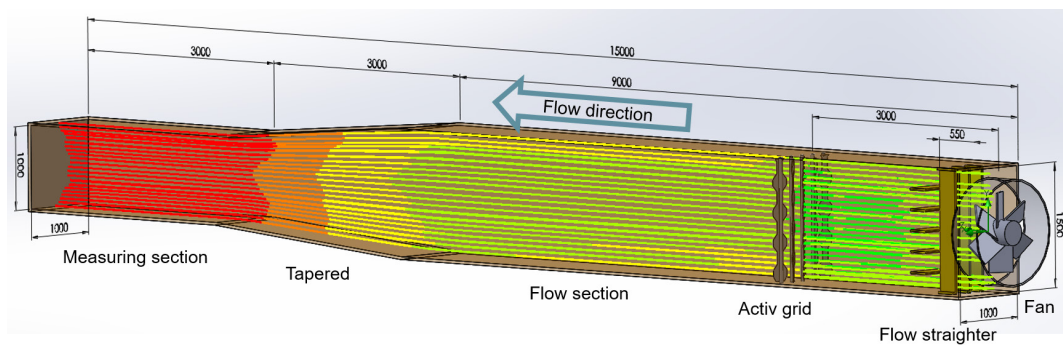


FIG. 4 Wind tunnel with flow simulation

For powering the wind tunnel, an axial ventilator of type MGV-LB 125 / 100FD was used with axial thrust of approx. 2600 Pa and air output of 210,000m<sup>3</sup>/h. The propellers have six blades and are reinforced with carbon fibre.

To reduce the swirl from the ventilator, a flow straightener was installed after it. The grid structure breaks up the rotation of a spinning air mass, thereby producing a straightened flow.

Wind gusts are produced in the wind tunnel by means of an active grid (Kroger et al., 2018). In this prototype, a uniaxial, continuously rotating active grid was designed for simplicity. The active grid consists of five octagonal, honeycomb-shaped chrome steel plates. The gusts in the wind profile are generated using three plates with the same orientation (see Figure. 5). When the axles are rotated at 19 revolutions per minute, the wind tunnel is partially blocked for a brief instant, causing the airstream to back up in front of the active grid. When this momentary partial blockage is opened, the backed-up dynamic pressure streams through the tunnel in the form of a gust.

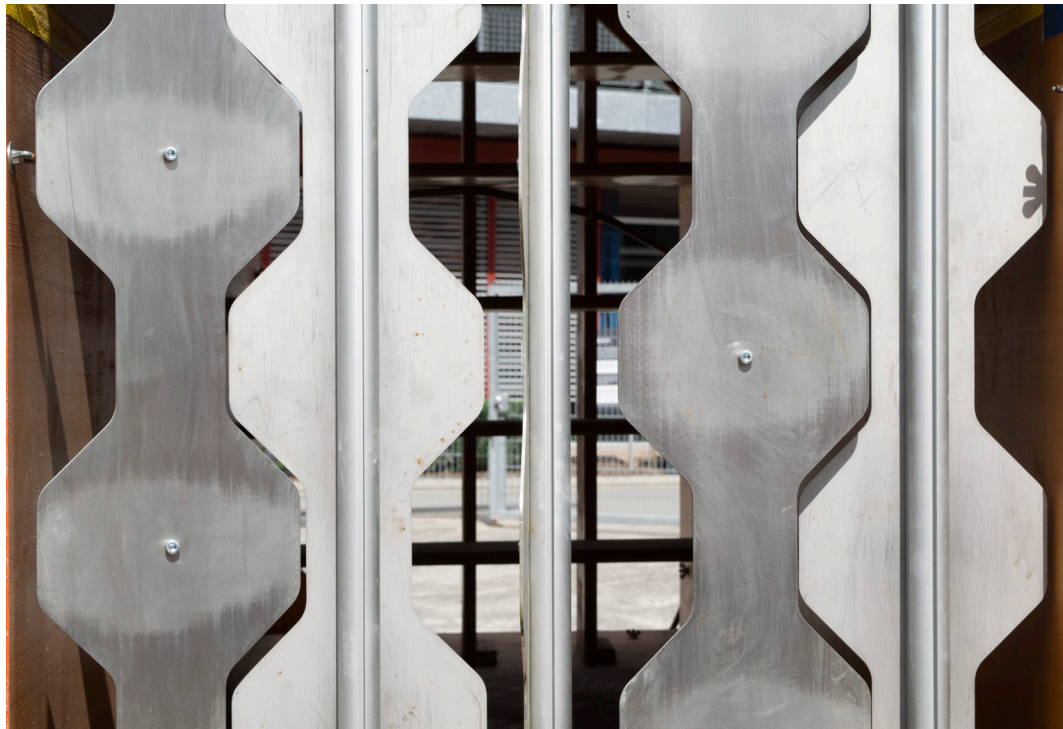


FIG. 5 Active grid for gust production in the wind tunnel

## 2.3 MEASURING EQUIPMENT

In the middle of the measuring section, three measuring stations for mounting samples are arranged one after another with a separation of 250mm. The ropes with the samples are attached on a sliding rail using horizontal, ball-bearing-mounted bearings. The flow forces of the samples are measured horizontally at each bearing by a corresponding force sensor S9M (500N) from HBM located above and below. The change in the rope force is measured by a further force sensor S9M (2000N) from HBM after the clamp connection on the upper bearing (see Figure. 6).

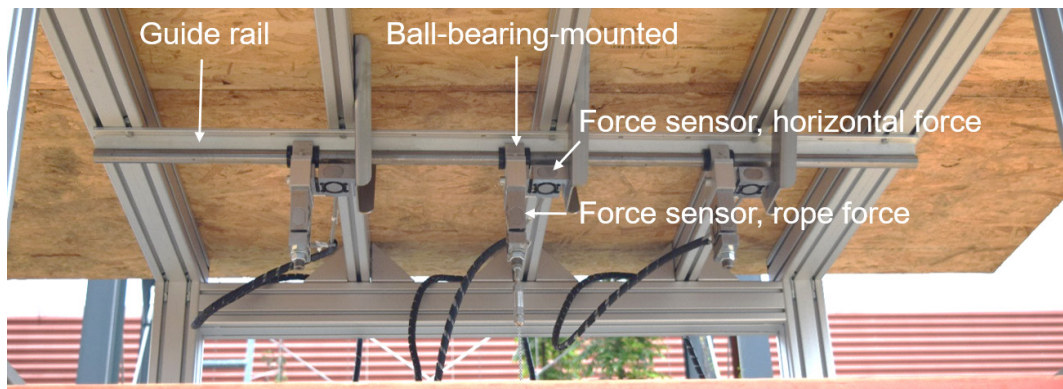


FIG. 6 Upper mounting for force measurement with bearings and force sensors

The force measurement data are recorded using a programmable logic controller (PLC). In order to detect the high frequencies of the vortices, data are recorded with a sampling rate of 2000 Hz.

By removing the honeycomb-shaped octagonal plates in the active grid, a second flow profile is generated in the wind tunnel. With the active grid, a flow profile with high turbulence (flow profile 1) is produced in the wind tunnel. Without the active grid, a flow profile with low turbulence (flow profile 2) is produced. These two flow profiles were measured using a two-dimensional ultrasonic anemometer with a sampling rate of 200 Hz at 15 positions in the plane in the middle of the 3m measuring section at different speeds (see Figure. 7).

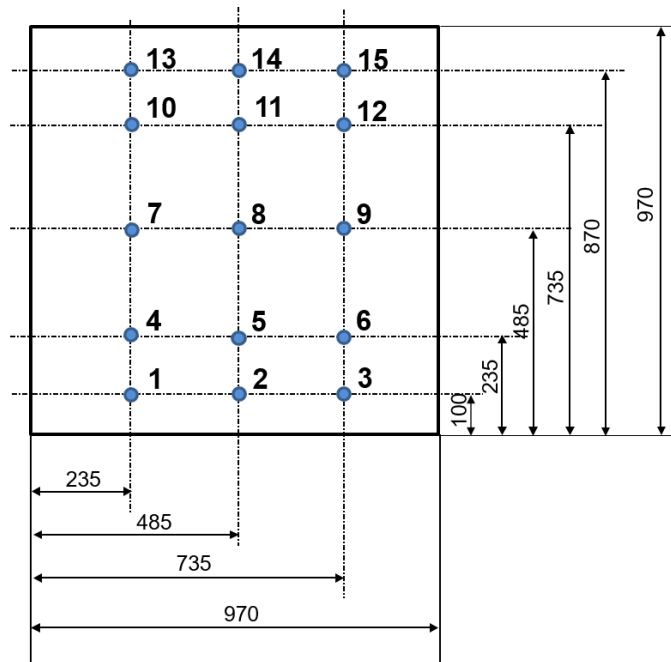


FIG. 7 Left: ultrasonic anemometer; Right: measuring points in flow profile, dimensions in mm

The measured speeds for the flow profiles were evaluated by determining at each speed level and measuring point the average speed  $v_m$ , the standard deviation  $\sigma$ , the turbulence intensity  $I$  according to formula (2.3), the peak speed  $\hat{v}$ , and the gust factor  $G_v$  by rearranging formula (2.2). Each average value was formed over the measuring points. The two flow profiles are shown in Table 1 with the corresponding parameters.

TABLE 1 Flow speed measurement for flow profiles 1 & 2

FLOW PROFILE 1 (HIGH DEGREE OF TURBULENCE)					FLOW PROFILE 2 (LOW DEGREE OF TURBULENCE)				
$v_m$ [m/s]	$\sigma$ [m/s]	$I$ [%]	$\hat{v}$ [m/s]	$G_v$ [-]	$v_m$ [m/s]	$\sigma$ [m/s]	$I$ [%]	$\hat{v}$ [m/s]	$G_v$ [-]
6.32	0.57	9.03	7.91	1.25	8.82	0.21	2.44	9.73	1.10
12.34	1.63	13.18	16.96	1.37	12.35	0.24	1.94	13.54	1.10
19.58	3.12	15.9	27.94	1.43	19.87	0.35	1.77	21.12	1.06
N/A	N/A	N/A	N/A	N/A	30.59	0.54	1.77	32.93	1.08

## 2.4 VALIDATION OF MEASUREMENT SETTING

The bearings in the measuring stations are mounted using ball bearings for low friction. Due to the pre-tensioning force of the ropes as well as the rope force that results from the wind load, potential friction forces arise in the bearings that influence the measurement. This friction was measured and the result was used to calculate appropriate coefficients of friction for each applied force. These coefficients of friction were then entered into the evaluation of the measurement results.

For validation of the wind tunnel, a comparison measurement was performed for both flow profiles on a 1m cylindrical PVC tube with a diameter of 100mm. The drag coefficients determined in this manner are listed in Figure 8, where they are compared on the basis of the Reynolds number with known drag coefficients for comparable cylinders in a laminar flow (Jirka, 2007).

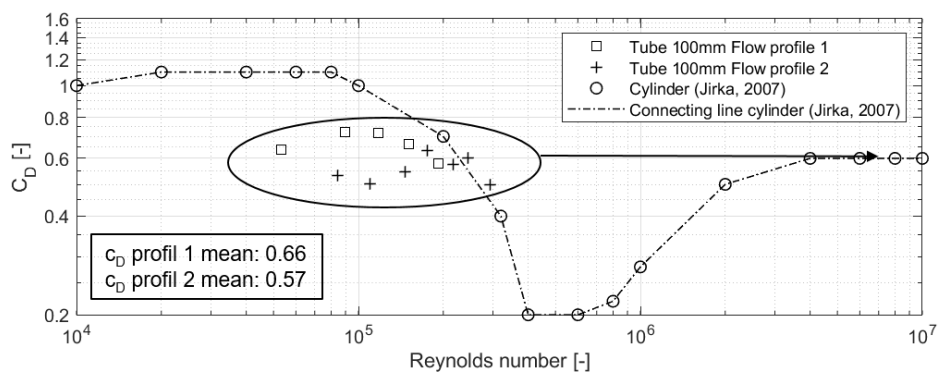


FIG. 8 Comparison measurement of a tube (d=100mm) for wind tunnel verification

For Reynolds numbers between  $3 \cdot 10^5$  and  $10^6$ , cylinders exposed to a laminar flow experience a local minimum of the drag coefficients at which the flow around the cylinder changes from laminar to turbulent (see "Connecting line cylinder" in Figure 8).

As the mean value, a drag coefficient of 0.66 was obtained in the comparison measurement for cylinders in flow profile 1 and a drag coefficient of 0.57 in flow profile 2. For Reynolds numbers in the range  $> 3 \cdot 10^6$ , the flow around cylinders is fully turbulent exposed to a laminar flow. In a fully turbulent flow, the cylinders attain drag coefficients of 0.6 (Jirka, 2007). The measured drag coefficients from the comparison measurement can be compared based on the turbulent flow profile with the drag coefficients of the cylinder with a value of 0.6 in a turbulent flow. On average, they diverge by 0.06 and 0.03. However, these divergences are greater at slow flow speeds in the wind tunnel than at the maximum values. The measuring system is validated by this comparison measurement. Through the turbulent flow profile, drag coefficients are attained for cylinders with values close to 0.6.

### 3 MEASUREMENT AND EVALUATION METHODOLOGY

#### 3.1 DETERMINATION OF THE PROJECTION AREAS

As shown in the first part of the study by Arnold et al. (2021), the projection area of the plants must be determined in the stationary state. The plant samples were photographed in front of a black cloth and pixelated. For scaling of the pixels, the area of the wind tunnel cross-section was marked on the cloth. The projection areas of the samples were recorded prior to the test run from two sides offset by 90 degrees. Based on a greyscale image and a subsequently generated black-and-white image, the representations of the samples were separated from the black background using Matlab software (see Figure 9). The area of a pixel is equal to  $A/n$ , where  $n$  is the total number of pixels within the marked area  $A$  of the wind tunnel dimension. The projection area of a given sample can be determined by counting the number of white pixels and multiplying this number by the area of a pixel. In the evaluation, the average value of the two determined projection areas per sample is used.

The calculation of the projection areas is checked once per plant using 1:1 print-outs in a process in which the plant and background are separated and the corresponding paperweights are determined. The check of the *Lonicera henryi* sample was used for specification of the assignment limit for the pixels in the greyscale image. This assignment limit is used to define which pixels in the greyscale image should be counted as black pixels and which as white pixels.

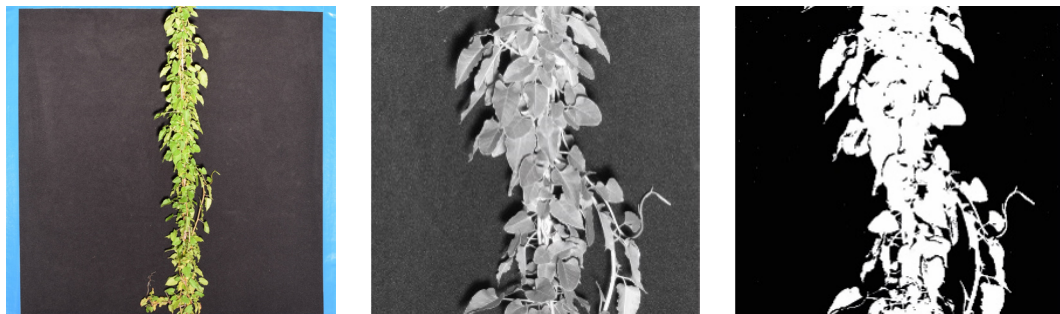


FIG. 9 Determination of the projection areas of the samples: (left) sample photograph, (middle) greyscale image, and (right) black-and-white image

## 3.2 WIND TUNNEL MEASUREMENTS

The wind tunnel provides “flow profile 1” and “flow profile 2”. Flow profile 2 exhibits lower turbulence intensities compared to flow profile 1, whereby the influence of the turbulence in the flow can be detected based on possible differences in the drag resistance measurement. Through the addition of water in “Flow profile 1”, another flow profile was created in the wind tunnel, which is designated as “Flow profile 1 with rain”. This profile corresponds to a thunderstorm with rain, thus allowing a measurement of the influence of rain on the plants. The influence of “rain” in the flow on the drag resistance of the plants can be measured by comparing the drag resistance values with the corresponding values for flow profile 1. The three flow profiles are described in Table 2.

TABLE 2 Different flow profiles in the study

<b>Flow profile 1</b>	Gusty flow with high degree of turbulence of up to 15.9% due to the active grid. This flow profile simulates the dry airflow of the wind prior to a storm without rain.
<b>Flow profile 1 with rain</b>	Gusty flow with high degree of turbulence of up to 15.9% due to the active grid with rain*. This flow profile simulates a storm with rain and strong winds.
<b>Flow profile 2</b>	Straightened flow with low degree of turbulence of up to 2.44% using the ventilator without the active grid. This flow profile does not occur in nature. However, this flow profile produces the highest speeds.

\* In addition, the water volume for the water tightness test for façades (EN 12155) of  $2l/min \cdot m^2$  is introduced into the wind tunnel in the straightener using water spray nozzles.

Two series of tests were performed: In a first series of tests, the drag resistance values were measured for all samples with flow profile 1. Following this first series of tests, the samples did not exhibit any major loss of leaves, meaning they could be used for a second series of tests. The samples were divided into two groups for the second series of tests. In the second series of tests, wind load tests were performed on a half of all samples (even-numbered plants: see Table 4) with flow profile 1 with rain. The drag resistance values were measured with flow profile 2 for the other half (odd-numbered plants: see Table 4). Determination of the projection areas was carried out as described in section 3.1 prior to each series of tests.

In order to measure the drag resistance values for the plant samples over the speed range of the wind tunnel, the measurements were performed at the different flow speeds listed in Table 3. These measuring speeds were set based on the rotational speed of the ventilator, which was then held constant during the measurement. Prior to each measurement, the average flow speed was measured with a manual impeller anemometer over an interval of 15 seconds in the middle of the tunnel at a distance of 0.5m before the sample.

TABLE 3 Measuring speeds for the different flow profiles (average)

FLOW PROFILE	AVERAGE MEASURING SPEED [M/S]							
Flow profile 1	5.5	9	12	15	19	N/A	N/A	N/A
Flow profile 1 with rain	5.5	9	12	15	19	N/A	N/A	N/A
Flow profile 2	N/A	8.5	10.5	15	19	23	26	30

Using the three measuring stations, up to three samples could be measured one after another. In order to correctly capture the flow map for the three stations, the three stations were set up as follows: In the first measurement, a plant sample is mounted in the last measuring station in the direction of flow and its drag resistance is measured at the different measuring speeds. In this test position, a deformation sensor is additionally arranged in the middle of the rope, which determines the sag of the rope. Following this measurement, a second sample is mounted in the middle test position and all drag resistance values for both samples are measured at the different measuring speeds. In the third measurement, the third test position is used and the forces are measured for all three-test plants at the individual measuring speeds. The test sequence is illustrated in Fig. 10.

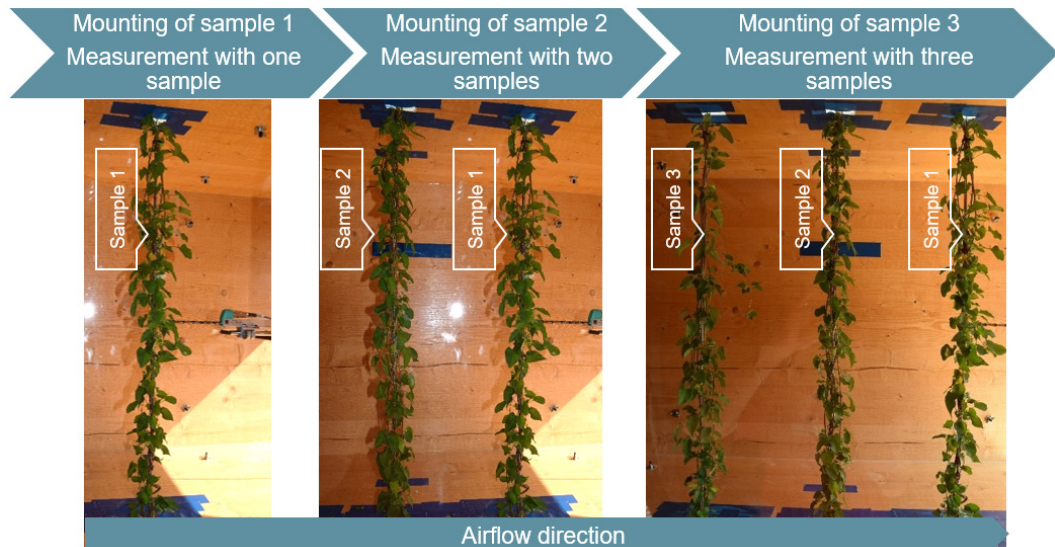


FIG. 10 Test sequence with successive mounting of the samples

### 3.3 EVALUATION SETTING FOR MEASUREMENTS

When performing a drag resistance measurement in a turbulent flow profile, a basic question that arises is whether the drag resistance values averaged over the time interval at averaged speeds are relevant, or the occurring peak force values at the peak speeds of the gusts. Based on the high-resolution measurement data for the force values and the high-resolution speed measurement of the flow profiles (see section 2.3), this basic question is resolved by evaluating the measurement data for both cases and comparing the results.

By adding the upper  $F_o$  and lower  $F_u$  force values, the total drag resistance of the sample is obtained. The frictional component for the bearings was determined by continuously increasing a force applied in the middle of the rope. The difference in the applied force with the total measured force of the measuring stations in this friction measurement is divided by the applied force to obtain the coefficient of friction  $\mu$  of the bearings. This coefficient of friction was taken into account in the evaluation for each measured force value. The total force is divided by the corresponding projection area  $A$  of the samples so that the forces can be compared with one another per area. According to formula (2.4), the averaged force  $F_{w,m}$  is thus obtained over the sample size  $n$  for each measuring speed.

$$F_{W,m} = \frac{\sum_{i=1}^n (F_{u,i} + F_{o,i}) \cdot (1 + \gamma_i) / A_i}{n} \quad [\text{N}] \quad (2.4)$$

Using the statistical method described in EN 1990, (2002), Annex D, the 5% characteristic value of materials can be determined in test-aided design. For determination of the wind loading forces on the plants, it is the upper 95% characteristic value in the statistical distribution that is critical (and not the lower 5% characteristic value). By adding, rather than subtracting, the standard deviation  $S_x$  multiplied by the factor  $k_n$ , the 95% characteristic value  $F_{W,q}$  based on the normal distribution can be calculated according to formula (2.5) from the average value  $F_{W,m}$  of the different drag resistances of the sample size per plant type. The factor  $k_n$  is dependent on the sample size and is documented in EN 1990 (2002).

$$F_{W,q} = F_{W,m} + k_n \cdot s_x \quad [\text{N}] \quad (2.5)$$

In order to allow better comparison of the measurement data, the individual data points as well as the calculated statistical characteristic values were subjected to the least-square interpolation in the diagrams of the results in section 4.2. A polynomial function 2<sup>nd</sup> degree according to formula (2.6) was selected. The minimum sample size for the statistical evaluation according to EN 1990 (2002) is  $n = 3$ . Since three samples were not available for all of the test runs, the 95% characteristic value of the drag resistances could not be determined everywhere.

$$F = a \cdot v + b \cdot v^2 \quad [\text{N}] \quad (2.6)$$

The quality of the curves is checked based on the residuals. Residuals represent the absolute value of the difference between the measuring point and the average for the sample size. The curves of the drag resistances  $F$  from the different flow profiles are compared with one another. Based on this comparison, the flow profile with the highest drag resistance values was determined. Based on the statistical drag resistance values for flow profile 1 and flow profile 1 with rain, the drag coefficients were calculated according to formula (2.7). Using flow profile 2, it was possible to obtain test data at higher speeds. However, this involves the side effect of a low-turbulence flow that does not occur in nature. The drag resistance values for flow profile 2 are documented for comparison purposes. However, no drag coefficients were calculated from these values.

$$c_{D(\hat{v})} = \frac{2 \cdot F_{W,q}}{\rho_L \cdot \hat{v}^2} \quad [-] \quad (2.7)$$

The course of the function of the drag coefficient  $c_d$  is characterised in formula (1.1). The calculated drag coefficients for the individual measuring speeds were interpolated using the least-square method and the specification of the power function according to formula (1.1). Through this interpolation, specific functions for the drag coefficients were obtained for each plant type. Through the B-values and E-values from the first part of the study, the drag resistance values

can be determined for use in planning overgrown rope façades with formula (2.8) according to Arnold et al. (2021).

$$F_w = B \cdot v^E \cdot A \cdot \frac{\rho \cdot \hat{v}^2}{2} = B \cdot A \cdot \frac{\rho \cdot \hat{v}^{2+E}}{2} \quad [N] \quad (2.8)$$

In the diagrams of the drag coefficients in the results in section 4.5, the drag coefficient from Arnold et al. (2021) is plotted for comparison purposes. Since the tests with this resultant drag coefficient were carried out on deciduous trees in a laminar flow, it was necessary to transform this function to the peak speed range using the gust factor of 1.9 (Hertig & Zimmerli, 2006). This transformation was realised by dividing the function into individual data points. The speed value for each data point was multiplied by the gust factor. Then, the data points transformed to the peak speed range were interpolated using the least-square method.

### 3.4 SPECIMEN PREPARATION AND CHARACTERISTICS OF THE SAMPLES

In order to carry out tests on climbing plants, the plants are required needed in a sufficiently advanced stage of growth. Accordingly, the climbing plants were selected based on specific cultivation of the samples in a very early stage. For the tests, samples of five species of climbing plants were chosen: evergreen honeysuckle "Lonicera henryi", silver lace vine "Fallopia aubertii", ivy "Hedera hibernica", Amur grape "Vitis amurensis," and Chinese wisteria "Wisteria sinensis". Two specimens were planted per plant species. From each specimen, three plant samples were raised on ropes, whereby six samples were available on rope lines per plant species. For some plants, it was not possible to cultivate al six -rope lines during the two-year growth cycle, resulting in gaps in the photographic catalogue of the samples in Table 4.

TABLE 4 Tested samples per plant species with sample numbers

SAMPLES FOR FLOW PROFILE 1 AND FLOW PROFILE 2			SAMPLES FOR FLOW PROFILE 1 AND FLOW PROFILE 1 WITH RAIN		
<b>Lonicera henryi</b>			<b>Lonicera henryi</b>		
Sample 1.1	Sample 1.2	Sample 1.3	Sample 2.1	Sample 2.2	Sample 2.3
					
<b>Fallopia aubertii</b>			<b>Fallopia aubertii</b>		
Sample 3.1	Sample 3.2	Sample 3.3	Sample 4.1	Sample 4.2	Sample 4.3
					
<b>Hedera hibernica</b>			<b>Hedera hibernica</b>		
Sample 5.1	Sample 5.2	Sample 5.3	Sample 6.1	N/A	N/A
					
<b>Vitis amurensis</b>			<b>Vitis amurensis</b>		
Sample 7.1	Sample 7.2	N/A	Sample 8.1	Sample 8.2	Sample 8.3
					
<b>Wisteria sinensis</b>			<b>Wisteria sinensis</b>		
Sample 9.1	Sample 9.2	Sample 9.3	Sample 10.1	Sample 10.2	Sample 10.3
					

## 4 RESULTS

### 4.1 PROJECTION AREAS

Table 5 lists the projection areas for all samples for the measurements in flow profile 1 of the first series of tests.

TABLE 5 Projection areas for the first series of tests

NO.	AREA [m <sup>2</sup> ]	NO.	AREA [m <sup>2</sup> ]						
1.1	0.070	3.1	0.073	5.1	0.060	7.1	0.045	9.1	0.290
1.2	0.111	3.2	0.086	5.2	0.065	7.2	0.175	9.2	0.177
1.3	0.047	3.3	0.049	5.3	0.089			9.3	0.079
2.1	0.088	4.1	0.072	6.1	0.100	8.1	0.211	10.1	0.172
2.2	0.104	4.2	0.063			8.2	0.171	10.2	0.064
2.3	0.078	4.3	0.053			8.3	0.126	10.3	0.152

Table 6 lists the projection areas for all samples for the measurements in flow profile 1 with rain and flow profile 2 of the second series of tests.

TABLE 6 Projection areas for the second series of tests

NO.	AREA [m <sup>2</sup> ]	NO.	AREA [m <sup>2</sup> ]						
1.1	0.053	3.1	0.063	5.1	0.052	7.1	0.040	9.1	0.245
1.2	0.097	3.2	0.076	5.2	0.069	7.2	0.165	9.2	0.165
1.3	0.052	3.3	0.047	5.3	0.076			9.3	0.070
2.1	0.078	4.1	0.063	6.1	0.084	8.1	0.194	10.1	0.145
2.2	0.084	4.2	0.057			8.2	0.158	10.2	0.063
2.3	0.062	4.3	0.054			8.3	0.100	10.3	0.157

The spot check of the projection area determination is documented in Table 7. Except for plant species 1.1 (sample for calibration), deviations of different sizes are apparent in the projection areas determined from the photographs using Matlab.

TABLE 7 Spot check of the projection area determination

PLANT	NO.	AREA CONTROL [m <sup>2</sup> ]	AREA MATLAB [m <sup>2</sup> ]	DEVIATION [%]
Lonicera henryi	1.1 Photo 1	0.069	0.069	0
Fallopia aubertii	3.2 Photo 1	0.080	0.074	7.3
Hedera hibernica	5.3 Photo 2	0.101	0.069	31.5
Vitis amurensis	8.1 Photo 1	0.220	0.209	5.3
Wisteria sinensis	9.1 Photo 2	0.170	0.143	16.4

## 4.2 FLOW RESISTANCE OF THE PLANT SAMPLES

Comparison of the test data for force values averaged over the time interval at averaged speeds with peak force values at peak speeds revealed that the samples exhibited higher peak force values at peak speeds versus averaged speeds with averaged force values. The peak speed of the gust produced higher drag resistances, whereby the calculated peak force values for the samples were evaluated per plant species at peak speeds in Figure 12 to Figure 16. The test data are shown in these diagrams for the different flow profiles. The individual data points are plotted by means of symbols (legend shown in Figure 11).

- |   |                          |   |   |
|---|--------------------------|---|---|
| + | Flow profile 1           | □ | Flow profile 1 95% characteristic value           |
| * | Flow profile 1 with rain | ◇ | Flow profile 1 with rain 95% characteristic value |
| X | Flow profile 2           | ○ | Flow profile 2 95% characteristic value           |

FIG. 11 Legend of the measuring points of Figure 12 to Figure 16

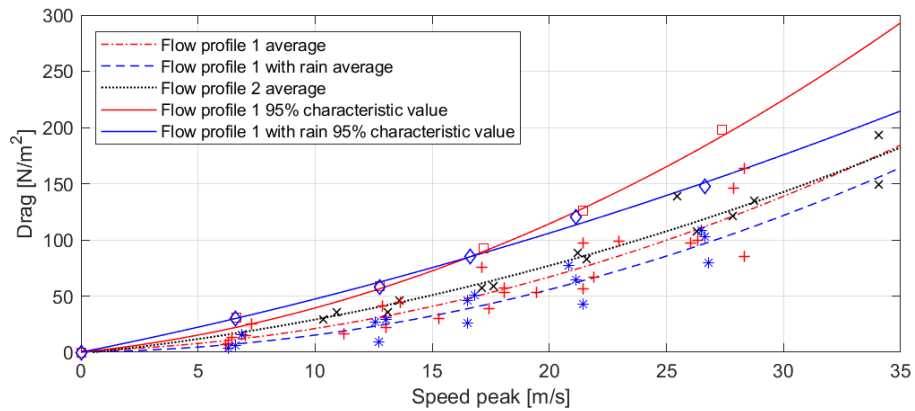


FIG. 12 Flow resistance of *Vitis amurensis*

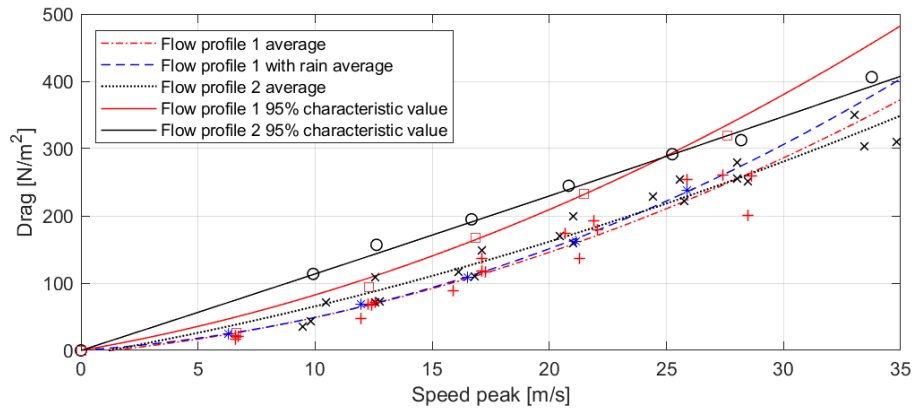


FIG. 13 Flow resistance of Hedera hibernica

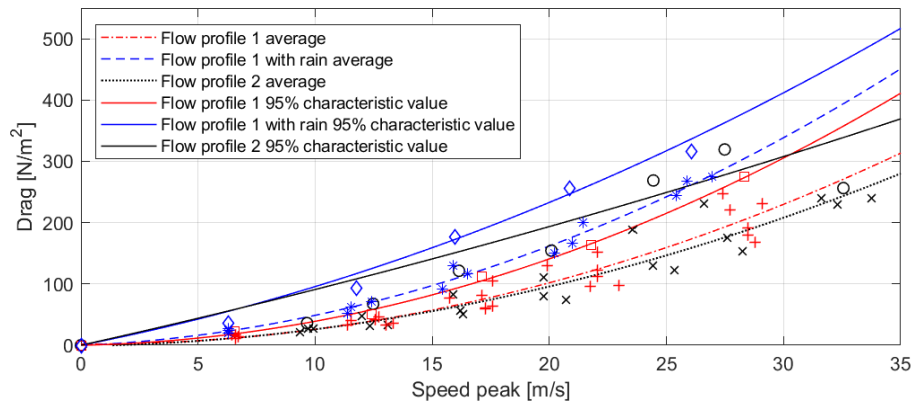


FIG. 14 Flow resistance of Lonicera henryi

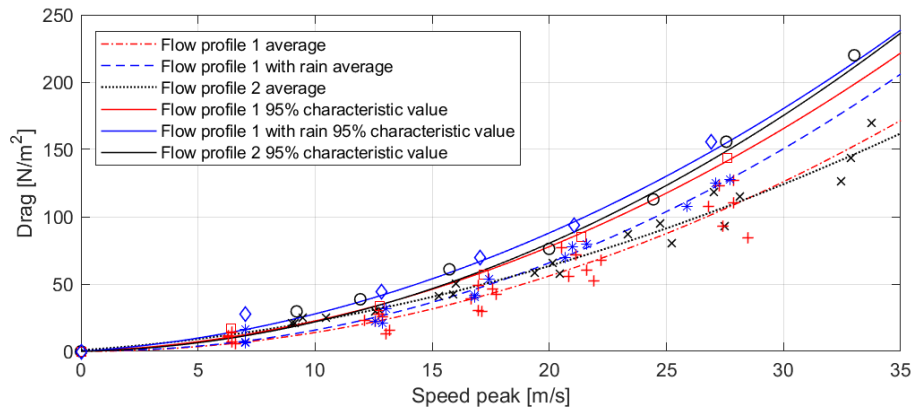


FIG. 15 Flow resistance Wisteria sinensis

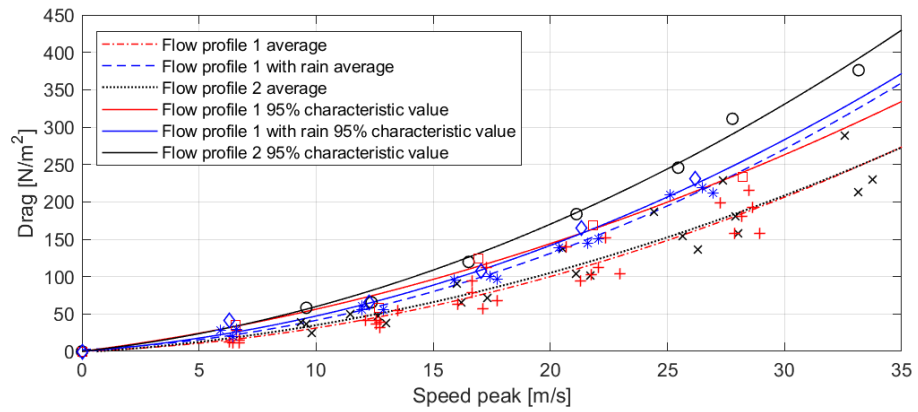


FIG. 16 Flow resistance *Fallopia aubertii*

Comparison of the different flow profiles (Figure 12 to Figure 16) shows that maximum forces are attained for the statistical 95% characteristic value in the speed range from 30m/s to 35m/s for flow profile 1 and flow profile 1 with rain for two plants in each case (Figure 12 and Figure 13, Figure 14 and Figure 15). For flow profile 2, only the plant type *Fallopia aubertii* attains maximum drag resistance values for the statistical 95% characteristic value (Figure 16). Overall, flow profile 1 with rain attains the highest resistance values of the averaged force values for four plants (Figure 13 to Figure 16).

### 4.3 RESIDUALS

As an example of the evaluation of the residuals, Figure 17 shows the residuals for the plant *Wisteria sinensis* with flow profile 1. The residuals for the other plants exhibit the same behaviour and increase at higher speeds.

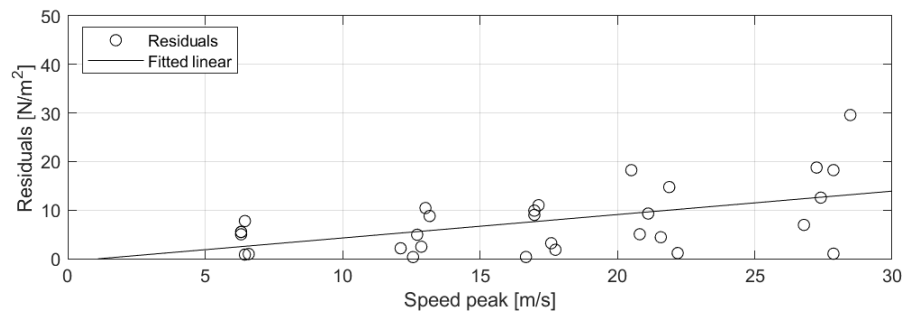


FIG. 17 Residuals of *Wisteria sinensis*

## 4.4 DRAG COEFFICIENTS

Based on the calculated 95% characteristic values of the drag resistances, the drag coefficients were determined according to formula (2.7) for flow profile 1 and flow profile 1 with rain. The calculated drag coefficients were interpolated based on the power function according to formula (1.1) in Figure 18 and Figure 19.

The drag coefficient from Arnold et al. (2010) transformed to the peak speed range assumes the function value  $5.88 \cdot \hat{v}^{-0.634}$  in the peak speed range (see formula (4.1)).

$$3.92 \cdot v^{-0.63} \hat{=} 5.88 \cdot \hat{v}^{-0.634} \quad (4.1)$$

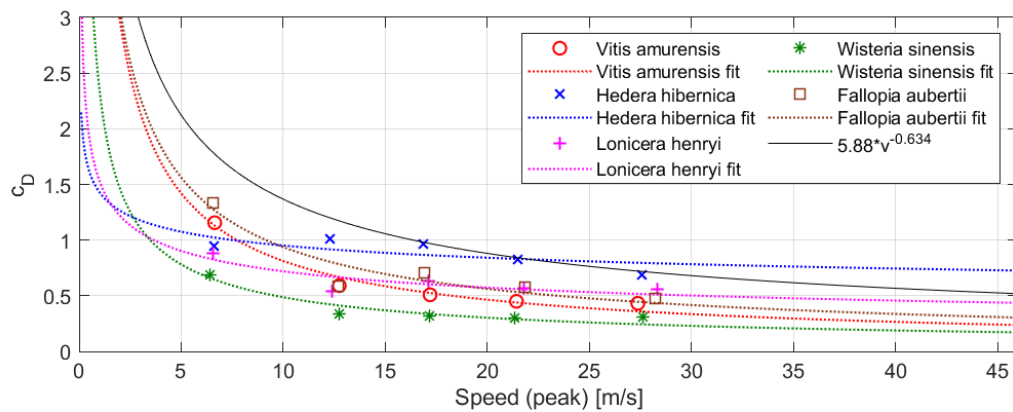


FIG. 18 Drag coefficients of flow profile 1

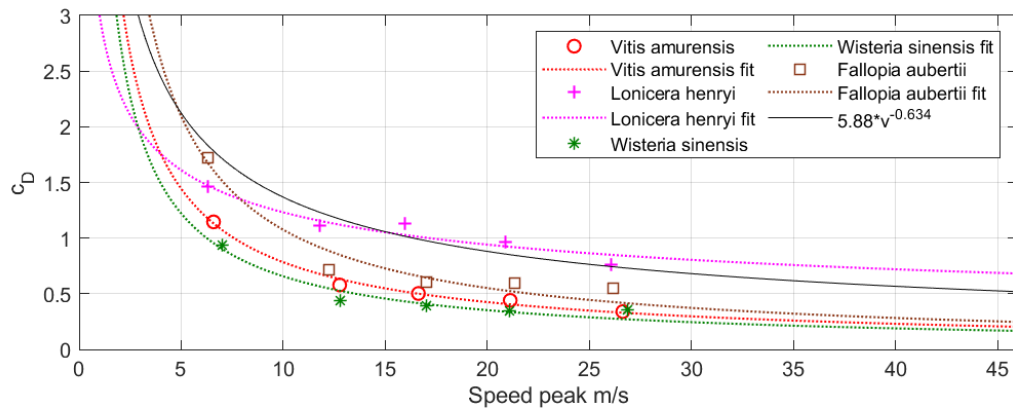


FIG. 19 Drag coefficients of flow profile 1 with rain

The function values of the drag coefficients for the studied plant species are listed in Table 8 for flow profile 1 and flow profile 1 with rain.

TABLE 8 Drag coefficients of the species

SPECIES	C <sub>D</sub> FLOW PROFILE 1	C <sub>D</sub> FLOW PROFILE 1 WITH RAIN
Vitis amurensis	$5.187 \cdot \hat{v}^{-0.805}$	$5.956 \cdot \hat{v}^{-0.880}$
Hedera hibernica	$1.429 \cdot \hat{v}^{-0.177}$	N/A
Lonicera henryi	$1.530 \cdot \hat{v}^{-0.327}$	$3.002 \cdot \hat{v}^{-0.387}$
Wisteria sinensis	$2.344 \cdot \hat{v}^{-0.682}$	$5.159 \cdot \hat{v}^{-0.895}$
Fallopia aubertii	$5.113 \cdot \hat{v}^{-0.737}$	$9.847 \cdot \hat{v}^{-0.962}$
General	$5.88 \cdot \hat{v}^{-0.634}$	

## 5 DISCUSSION

### 5.1 PROJECTION AREA DETERMINATION

The largest deviation that was found in the random check of the projection areas occurred for the plant species *Hedera hibernica* (31.5% deviation). *Hedera hibernica* has very dark leaves that make it difficult to separate the plant area from the background. Therefore, some areas of the leaf surface were counted as part of the background. In all of the random checks of the projection areas, a larger projection area was determined compared to the computer-aided evaluation. The determination of the projection area is subject to uncertainty. Through the results in Table 7, smaller projection areas were determined based on calculations with Matlab, whereby a larger drag resistance is obtained in the evaluation of the results according to formula (2.4). Due to the smaller projection areas that were generally determined, this uncertainty leads to a safety margin for the determined drag coefficients.

### 5.2 WIND TUNNEL AND FLOW PROFILES

The prototype of a turbulent wind tunnel that was built achieved peak speeds of 28m/s for flow profile 1. For flow profile 2, the peak speed was 33m/s. These flow speeds are lower than the peak speeds of the reference value for the dynamic pressure occurring in Switzerland of 46m/s. For flow profile 1 with 15% turbulence intensities, the wind tunnel attains a gust factor  $G_v$  of 1.4. Flow profile 1 exhibits less turbulence and a significantly lower gust factor than the natural airflow "Wind" described in Hertig an& Zimmerl, (2006). A compromise was made for more speed at the expense of turbulence. The influence of the difference in the turbulence in the wind tunnel compared to the natural airflow is considered low since the determined drag resistances hardly differ from one another without statistical evaluation of flow profile 1 and flow profile 2 in Figure 12 to Figur. 16. The tests were all performed in a turbulent flow. The extent to which the drag resistances of plants in a laminar flow affects the plants cannot be determined based on this study. Since the degree of turbulence in this study exhibits a low influence on the drag resistances of the plants, it is likely that plants create a turbulent flow around themselves due to their fluttering leaves. The flow can change in a laminar flow even at low Reynolds numbers due to the fluttering of leaves.

making the flow profile irrelevant. Although the speeds and turbulence that were produced in the flow of the wind tunnel were too low, valuable insights could be gained into the behaviour of the plants in the wind flow.

### 5.3 EVALUATION OF THE MEASUREMENT DATA

The friction of the bearings was taken into account by the coefficient of friction. This coefficient changes due to the variable rope force. Although this behaviour was taken into account in the evaluation, the friction of the bearings can vary over the test time and thus lead to increased scattering of the force values.

Evaluation of the residuals revealed increasing values at higher speeds. Steadily increasing residuals versus speed imply an increase in the standard deviation at higher speeds. In generating the 95% characteristic value according to formula (2.5), the difference between the average value and quantile value always increased at higher speed by; extrapolations followed this trend.

Comparison of the flow profiles for the average force values  $F_{w,m}$  led to the conclusion that the highest drag resistances occurred in four of the five plant species for flow profile 1 with rain. For flow profile 2, interference effects can possibly occur due to the low degree of turbulence since the samples exhibited partial tearing of their leaves (breaks in the centre of the leaf) at a peak speed of 32m/s. For flow profile 1, no noticeable leaf tearing was observed at the highest peak speed of 28m/s. It is not possible to state based on the test results whether leaf tearing also occurs for flow profile 1 at a peak speed of 32m/s.

The additional water drops in flow profile 1 with rain led to a higher density of the medium. The water drops adhering to the plants and leaves can further increase the drag on the flow around the individual leaves leading to generally higher drag resistance being obtained due to the presence of water in the flow medium.

Comparison of the flow profiles at the 95% characteristic values  $F_{w,q}$  is more difficult. Due to the different sample size of the second series of tests compared to the first series, the  $k_n$  values differ according to EN 1990 (2002). For a smaller sample size, the  $k_n$  values are greater; the higher differences compared to the average value and thus higher characteristic values are calculated according to formula (2.5)

In order to determine practical, design-relevant drag coefficients on the basis of wind load tests, statistical evaluation of the drag resistances versus the sample size is absolutely essential since characteristic resistance values averaged over the sample size do not conform to the design concept formulated in SIA 260 (2013).

### 5.4 DRAG COEFFICIENTS

In Figure 18, the plant species *Hedera hibernica* exceeds the drag coefficient of  $5.88 \cdot \hat{v}^{-0.634}$  that was derived based on deciduous trees, while in Figure 19 the plant species *Lonicera henryi* exceeds the same drag coefficient. Considering the individual data points for these two samples, it can be seen that the drag coefficients for these samples lie above the interpolated curve in the speed range from 10m/s to 20m/s. These higher resistance values could result from the stiffer leaves and

stems at low speeds. When exposed to wind, the leaves of the plants align themselves along the direction of the wind. In case of stiff leaves and leaf stems, significantly higher resistance forces are generated during this alignment phase at slow speeds. The leaves position themselves in the wind during the alignment phase. This increases the projection area, which consequently leads to higher drag coefficients. If all leaves are aligned along the flow direction, the drag force decreases. This "dynamic" projection area of plants with stiff leaves and stems leads to higher drag coefficients at slow speeds compared to the interpolated curve. This phenomenon is known in fir trees (Rudnicki et al., 2004). These higher resistance values in the slow speed range have a significant influence on the course of the interpolated curve by meaning that the curve is higher in the extrapolated range. In order to minimise the influence of this phenomenon of leaf alignment, drag resistance studies are needed up to the applicable peak speed in Switzerland of 46m/s. The uncertainty of the project area determination according to section 5.1 for the plant species *Hedera hibernica* of 31.5% deviation leads to a higher drag coefficient in this check. If this deviation were to be taken into account, the drag coefficient of *Hedera hibernica* in Figure 18 would shift evenly downwards. Therefore, it will be below the drag coefficient of  $5.88 \cdot \hat{v}^{-0.634}$ . The individual measuring points in the speed range from 10m/s to 20m/s would still be above the interpolated curves.

In the tests, a low degree of leaf tearing was encountered up to the maximum ventilator power for flow profile 1 and flow profile 1 with rain, though the effect of leaf tearing is not taken into account in the test data of this study. Due to the effect of leaf tearing, smaller drag coefficients are presumed in the speed range over 30m/s compared to what is forecast in this study based on extrapolations.

The drag coefficient derived by Arnold et al., (2021) on the basis of deciduous trees can be classified in relation to the test results as a conservative value on the safe side. For plant types that were not studied, it is still valid. The drag coefficients follow the power function  $C_D = B \cdot \hat{v}^E$  with negative E-values, by whereby the quadratic speed term is reduced by the E-value. The decrease in the projection area is taken into account at higher speeds by the E-value.

## 6 CONCLUSION

In this study, drag coefficients of five climbing plants were obtained based on the throughput. These drag coefficients were determined in a turbulent wind tunnel and can be determined object-specifically by power functions for each occurring speed at the building. The power functions are based on B-value and E-value values. The E-value reduces the quadratic velocity term according to Bernoulli, thus taking into account the orientation of the leaves and consequently the reduction of the projection area with increasing velocity with this constant.

The measurement results prove that the power function  $3.92 \cdot v^{-0.63}$  from Arnold et al., (2021) is on the safe calculation side. In the study, *Hedera hibernica* and *Lonicera henryi* were examined, which have very stiff leaves for climbing plants and therefore also have the highest drag coefficients. Thus, it can also be applied to climbing plant species which are not measured in this study. The wind speeds in the design of forces on building components according to SIA 261, (2014) or EN 1991-1-4, (2010) are considered as peak speeds in the measurements of this study. It is therefore important to use the function  $5.88 \cdot \hat{v}^{-0.634}$  (see formula (4.1)), which has been transformed into the peak speed range, to calculate the drag coefficient for climbing plants of overgrown rope façades.

Furthermore, various methods and test equipment had to be developed in this work, such as the photographic determination of the projection surfaces or air resistance measurements of plants on ropes, and a turbulent wind tunnel with an active grid. Some essential lessons learned of these developments are concluded in the following.

The determination of the projection area is subject to uncertainty, resulting in the calculation of areas that were too small. It is possible to minimise this uncertainty by taking photographs with a white background. The problem with this method lies in the shadowing that occurs, meaning that the photographs should be taken with indirect lighting.

The friction influences of the bearings in the wind tunnel can be eliminated using a different mounting system in which the samples are mounted in a frame. The rope tension is eliminated in this frame and thus does not influence the frame with its low-friction mounting.

In order to investigate the phenomenon of leaf loss in the plants, the wind tunnel needs higher speeds. Since the expected forces are now known, the sensor technology can be optimally configured in future. By optimising the mounting conditions, the influence of friction is minimised and results that are more accurate can be obtained.

In order to obtain a complete overview of the wind loading behaviour of climbing plants, the study must be extended to further species of climbing plants. Since 2017, samples of 14 climbing plants have been cultivated at Lucerne School of Engineering and Architecture for this purpose. The sample size was increased to nine samples per plant type in order to reduce the influence of the sample size in the statistical evaluation such that more dependable characteristic values can be expected.

In a subsequent study, the drag coefficients of all 14 climbing plants will be determined. Wind tunnel tests will again be required. Drag coefficients from wind tunnel tests are based on the throughput. The wind loading behaviour of overgrown rope façades on the building was not addressed in this study. This two-dimensional structure is influenced by the flow around the building, thereby entailing additional influence parameters. It is difficult to scale the plants in order to perform wind loading measurements in a boundary layer wind tunnel (Aly et al., 2013). A CFD simulation of an overgrown rope façade that exploits the characteristic of the determined drag coefficients of the plants can potentially produce promising results for ascertaining the wind loading behaviour of overgrown rope façades on buildings.

### **Acknowledgement**

The tests were carried out in the course of the main author's master's thesis. Special thanks go to Lucerne University of Applied Sciences and Arts (Lucerne School of Engineering and Architecture), which enabled the construction of the prototype of a turbulent wind tunnel and for its support in elaborating the results of this paper. Thanks also go to Jakob Rope Systems, who sponsored the rope structures and connections for the cultivation the samples.

## References

- Aly, A. M., Fossati, F., Muggiasca, S., Argentini, T., Bitsuamlak, G., Franchi, A., ... Chowdhury, A. G. (2013). Wind loading on trees integrated with a building envelope. *Wind and Structures*, 17(1), 69–85. <https://doi.org/10.12989/was.2013.17.1.069>
- Arnold, K. (2018). *Windkräfte auf bewachsene Seilfassaden* [Wind Force in overgrown rope façades]. [Master Thesis]. Lucerne University of Applied Sciences and Arts. <https://doi.org/10.5281/zenodo.1409485>
- Arnold, K., Gosztonyi, S., & Luible, A. (2021). Wind Forces in Overgrown Rope Façades: Drag Coefficient Suggestion for Climbing Plants Based on Study Review. *Journal of Façade Design & Engineering*. <https://doi.org/10.7480/jfde.2021.2.4831>
- Chanetz, B. (2017). A century of wind tunnels since Eiffel. <https://doi.org/10.1016/j.crme.2017.05.012>
- Cook, N. J. (1975). A boundary layer wind tunnel for building aerodynamics. *Journal of Wind Engineering and Industrial Aerodynamics*, 1, 3–12. [https://doi.org/10.1016/0167-6105\(75\)90003-3](https://doi.org/10.1016/0167-6105(75)90003-3)
- EN 1990. (2002). Eurocode: Basis of structural design. [Standard]. Europe
- EN 1991-1-4. (2010). Eurocode 1: Actions on structures - Part 1-4: General actions - Wind actions. [Standard]. Europe
- Hertig, J.-A., & Zimmerli, B. (2006). *Wind: Kommentar zum Kapitel 6 der Normen SIA 261 und 261/1 (2003): Einwirkungen auf Tragwerke* [Wind: Commentary on chapter 6 of the standards SIA 261 an 261/1 (2003): Actions on supporting structures]. SIA, Schweizerischer Ingenieur- und Architektenverein.Schweiz
- Jirka, G. H. (2007). *Einführung in die Hydromechanik* [Introduction to hydromechanics]. KIT Scientific Publishing.
- Kröger, L., Frederik, J., Wingerden, J.-W. van, Peinke, J., & Hölling, M. (2018). Generation of user defined turbulent inflow conditions by an active grid for validation experiments. *Journal of Physics: Conference Series*, 1037, 052002. <https://doi.org/10.1088/1742-6596/1037/5/052002>
- Pfoser, N. (2016). *Fassade und Pflanze. Potenziale einer neuen Fassadengestaltung* [Façade and plant. Potentials of a new façade design]. [Dissertation]. Technische Universität Darmstadt, Darmstadt, <https://tuprints.ulb.tu-darmstadt.de/id/eprint/5587>
- Pfoser, N. (2018). *Vertikale Begrünung*. [Vertical greening]. Stuttgart: Verlag Eugen Ulmer. ISBN 978-3-8186-0088-4
- Rudnicki, M., Mitchell, S. J., & Novak, M. D. (2004). Wind tunnel measurements of crown streamlining and drag relationships for three conifer species. *Canadian Journal of Forest Research*, 34(3), 666–676. <https://doi.org/10.1139/x03-233>
- SIA 260. (2013). Basis of structural design. [Standard]. Switzerland.
- SIA 261. (2014). *Einwirkungen auf Tragwerke* [Actions on supporting structures]. [Standard]. Switzerland